Peer-reviewed version available at *Materials* **2017**, *10*, 296; doi:10.3390/ma10030296

Article

Fabrication of Polymeric Antireflection Film Manufactured by Anodic Aluminum Oxide Template on the Dye-Sensitized Solar Cell

Jenn-Kai Tsai * and Yu-Shin Tu

Department of Electronic Engineering, National Formosa University, Yunlin 632, Taiwan; tuyushin993@gmail.com

* Correspondence: tsaijk@nfu.edu.tw; Tel.: +886-5-6315518, Fax: +886-5-6315643

Abstract: In this study, a high energy conversion efficient dye-sensitized solar cells (DSSC) was successfully fabricated by attaching a double anti-reflection (AR) layer which is composed of a subwavelength moth-eye structured polymethyl methacrylate (PMMA) film and a polydimethylsiloxane (PDMS) film. The efficiency is up to 6.79%. The moth-eye structured PMMA film was fabricated by using anodic aluminum oxide (AAO) template which is simple, low-cost and scalable. The nano-pattern of AAO template has been precisely reproduced onto PMMA film. The photoanode is composed of Titanium dioxide (TiO_2) nanoparticles (NPs) with diameter of 25 nm deposited on the fluorine-doped tin oxide (FTO) glass substrate and the sensitizer N3. The double AR layer can effectively improve the short-circuit current density (JSC) and conversion efficiency from 14.77 to 15.79 mA/cm^2 and from 6.26% to 6.79%, respectively.

Keywords: anodic aluminum oxide (AAO); subwavelength structure (SWS); antireflection; poly-methyl methacrylate (PMMA); dye-sensitized solar cell (DSSC); conversion efficiency

1. Introduction

Minimizing optical reflection in solar cells to improve conversion efficiency is always a major challenge. Literatures have shown that there are still more than 30% of the incident sunlight lost even with adopting antireflection (AR) film in the devices [1–3]. For example silicon nitride AR coating has been widely used in solar cells due to easily to fabricate; however, the performance is not satisfying due to its narrow-band and narrow-angle properties [4]. Multilayer AR film [4,5] also have been developed in order to further reduce the lost. However, its' process instability, high cost, and high-temperature procedure limit the applications of those AR films. Besides multilayer coating, surface texturization by alkaline etching technique is an alternative method that have been widely used in silicon based solar cell [6]. The idea arises from gradual variation in refractive index between air and silicon [6] that reduces the loss of light from reflection. Similar texturing technique using acid solution has also been applied to multi-crystalline silicon based solar cell. On the other hand, literatures have already found the subwavelength moth-eye structures for decades and have demonstrated that this structure has low reflection over a broad spectral range [7,8]. E-beam lithography, photolithography, and nano-sphere lithography techniques are available for fabricating moth-eye patterns [2]. However, these techniques are time consuming and expensive. Therefore, a cheap and efficient technique to fabricate moth-eye structured AR layer is needed for photovoltaic devices.

Grätzel et al. reported the dye-sensitized solar cell that has photoelectric conversion efficiency of 7.1% by using TiO_2 nano-porous electrode combined with dyes of metal ruthenium organic complexes and electrolyte containing I^-/I^{3-} redox couple [9]. Increasing photoelectric conversion efficiency and stability to achieve high performance dye-sensitized solar cell are the primary goals in this field. Major factors that influence the conversion efficiency are transparent conductive oxide (TCO), working electrode, sensitizer, electrolyte and counter electrode, etc., and optimization of those factors plays an important role. For example, the transparent conductive electrode must have at least

80% visible light transmittance, which limit the thickness of electro-conductive film. However, thick electro-conductive film is usually required in order to have sufficient conductivity.

In this paper, we propose a simple and cheap method to fabricate moth-eye structured additional AR layer that combined with DSSC device. The moth-eye structure was fabricated based on replication technology of anodic aluminum oxide (AAO) template. The additional AR layer was made by PMMA because of its high resolution, low cost and optical transparency in the wavelengths between visible and near-infrared regions. The additional PMMA AR films have gradual variation in refractive index that can effectively absorb incident light and greatly reduce the reflectivity [10]. Moreover, since the thin PMMA films are flexible, it can be mounted on curved optical structures for many interesting applications. Using PMMA or PDMS as anti-reflection layer on solar cell has been reported with great improvement on light harvest efficiency [10–13]. The efficiency increase can be up to 3%–5%. The process, however, needs heat treatment over 100 °C which is not compatible for the process to fabricate DSSC [14]. In this paper, we also developed a two-step process to overcome the issue.

2. Experimental

2.1. Fabrication of AAO Template

Super purity aluminum sheets （99.969%，Toyo Aluminium Foil, City, Japan）of 0.25 mm thickness were used as a substrate to serve as the original mold. The AAO template was fabricated by using two-steps anodization process. In the first anodization process, the pre-treated aluminum sheets were immersed to 0.1 M oxalic acid dihydrate (SIGMA-ALDRICH 99.5%, diluted by DI water) at a constant-voltage of 80 V and temperature of 4 °C for 3 h. During the anodization, the solution was stirred by a pump circulation system. Then, the anodic alumina layer was removed by wet chemical etching in 6 wt% phosphoric acid (H_3PO_4) with 1.8 wt% chromic acid (H_2CrO_4) at 60 °C for 60 min. The last anodization process was processed under the same conditions as the first anodization process, but the anodization period was reduced to 75 s. After that, the pore diameter of the anodic alumina was further widened by immersing the sample into 6 wt% phosphoric acid at 40 °C for 12 min.

2.2. Spin-Coating Replication

350 kmol, 15 wt% PMMA solution dissolved in toluene was spin coated on the AAO template at 1000 rpm rotation speed. The film then dried for 30 min at room temperature and baked at 200 °C in oven 30 min. The sample then immersed in 6wt% sodium hydroxide (NaOH) at 60 °C for 60 min to remove the AAO template. After that, the sample washed by dilute hydrochloric acid (10 %) and followed by drying in the oven at 45 °C for 10 min. At last, the subwavelength moth-eye structure PMMA film was been obtained.

2.3. DSSC Fabrication

10 wt% TiO_2 paste was prepared by mixing nanocrystalline TiO_2 particles (TG–P25, Degussa, Shinjuku, Tokyo, Japan; the average nanoparticle diameter was about 25 to 30 nm) with tert-butyl alcohol and deionized water. The TiO_2 paste was craped by doctor blading method on a transparent fluorine-doped-tin oxide (FTO) glass which has resistivity of 8 Ω/□. The sample then compressed mechanically at pressure of 279 kg/cm^2. The post heat treatment was done by two-step annealing, 150 °C for 90 min and 500 °C for 30 min in air, respectively to form TiO_2 photoanodes [15,16]. The 150 °C annealing temperature would decompose the residual organic compounds and the 500°C annealing temperature would assist the interconnection of TiO_2 NPs, so that the loss of electron transmission becomes less. The compressed and annealed TiO_2 NPs films were immersed in 0.3 mM N3 dye (cis-bis(dithiocyanato)-bis(4,4'-dicarboxylic acid-2,2'-bipyridine) ruthenium (II)) for 2 h. Subsequently rinsing in acetonitrile for a few seconds to wash out unbound dyes and drying in the oven at 45 °C. The counter electrode was made by electroplating of 1 nm thick Pt thin film on indium-tin-oxide (ITO) glass. The FTO substrate with TiO_2 NPs photoanodes and dye molecules on it were then flipped

Peer-reviewed version available at Materials 2017, 10, 296; doi:10.3390/ma10030296

and placed on Pt counter electrode with a 50 μm-thick hot-melt polymer spacer. Sealing was accomplished by pressing the two electrodes together at 115 °C for a few seconds. The redox electrolyte, consisting of 0.5 M LiI, 0.05 M I_2, and 0.5 M 4-tert-butylpyridine (TBP), and 1 M 1-propy1-2,3-dimethylimidazolium (DMPII) mixed into 3-methoxypropionitrile (MPN), was injected into the cell by capillary forces through an injecting hole that was previously made in the counter electrode by a drilling machine [17]. Finally, the hole was covered and sealed with a piece of hot-melt polymer to prevent leakage of the fluid-type electrolyte. The resulting active electrode area was approximately 0.25 cm^2 (0.5 cm × 0.5 cm).

At last, the photoanode side (where the incident light comes in) of the DSSC device was spin coated of Polydimethylsiloxane (PDMS) at 300 rpm for 15 sec and then 500 rpm for 20 sec. The PDMS solution was made by dissolving PDMS particle into DI water (weight ration of 1:10) with strong agitation. Then the PDMS solution was statically stored in vacuum chamber for one hour so that the tiny bubbles generated during stirring can eliminated. After spin coating of the PDMS film the subwavelength moth-eye structured PMMA film then attached onto the PDMS layer. The process should be very careful so that no air bubble was left at the interface. The device then dried at room temperature for 12 h. Figure 1 shows the structure of additional moth-eye subwavelength AR layer DSSC device that we have designed and fabricated in this study.

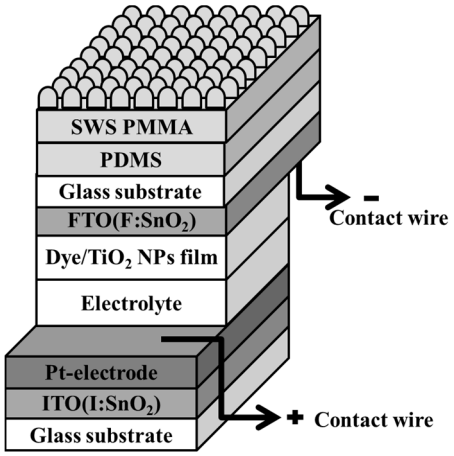

Figure 1. Structure diagram of a sub-wavelength structured (SWS) anti-reflective film combined on dye-sensitized solar cell.

2.2.4. Characterizations and Photoelectrochemical Measurement

The morphologies of PMMA film with subwavelength moth-eye structure were measured using the field-emission scanning electron microscope (FESEM; JSM-7500F, JEOL, Akishima-shi, Japan). The ultraviolet-visible (UV-Vis) transmittance spectrum of the PMMA film was observed by UV-Vis spectrophotometer (U-2900, Hitachi High-Technologies Corporation, Tokyo, Japan) with the wavelength ranging from 300 nm to 800 nm at room temperature. Electrochemical impedance spectroscopy (EIS; Zahner Zennium, Kronach, Germany) were performed in the frequency range from 10 mHz to 100 kHz under 1-sun (AM 1.5G) illumination (100 mW/cm^2) at an applied bias voltage and ac amplitude were set at open-circuit voltage of DSSC and 10 mV, respectively. The incident photon-to-current conversion efficiency (IPCE) were characterized by illuminating monochromatic light on the devices (with the wavelength from 300 to 800 nm). The light was generated by a 1000 W Xenon arc lamp which compose of a compact 1/8 meter monochromator (CM110, Spectral Products, Putnam, CT, USA), a color filter wheel (CFW-1-8, Finger Lakes Instrumentation, Lima, NY, USA), and a calibrated photodiode (FDS1010-CAL, Thorlabs Inc., Newton, NJ, USA) with Keithkey 2400 as source meter (Keithley Instruments, Inc., Cleveland, OH, USA). The current-voltage characteristics of samples were measured by Keithley 2400 source meter under a simulated sunlight (SAN-EI XES-40S1, San Ei Brand, Higashi-Yodogawa, Japan), AM 1.5 radiation at 100 mW/cm^2.

Peer-reviewed version available at Materials 2017, 10, 296; doi:10.3390/ma10030296

3. Results and Discussion

Figure 2 shows FESEM images of surface morphology of AAO template and subwavelength moth-eye structured PMMA film. Top-view image of AAO template showing in Figure 2a demonstrates that pore diameter of AAO template is around 110 nm. The cross-section image showing in Figure 2b indicates that pore depth of AAO template is about 238 nm. Figure 2c shows top-view image of PMMA film with subwavelength moth-eye structures made from rolling over of AAO template. The image indicates that top-end structure of PMMA is the same as AAO template with diameter around 110 nm. Figure 2d is a cross-sectional image of PMMA film. The height of PMMA moth-eye structure is about 234 nm which is also similar to the pore depth of AAO template. Due to capillary effect, some of the top-end moth-eye structure PMMA connect to each other with a thin line. Overall, the characteristic tubular pores of AAO template had been successfully copied to the PMMA film.

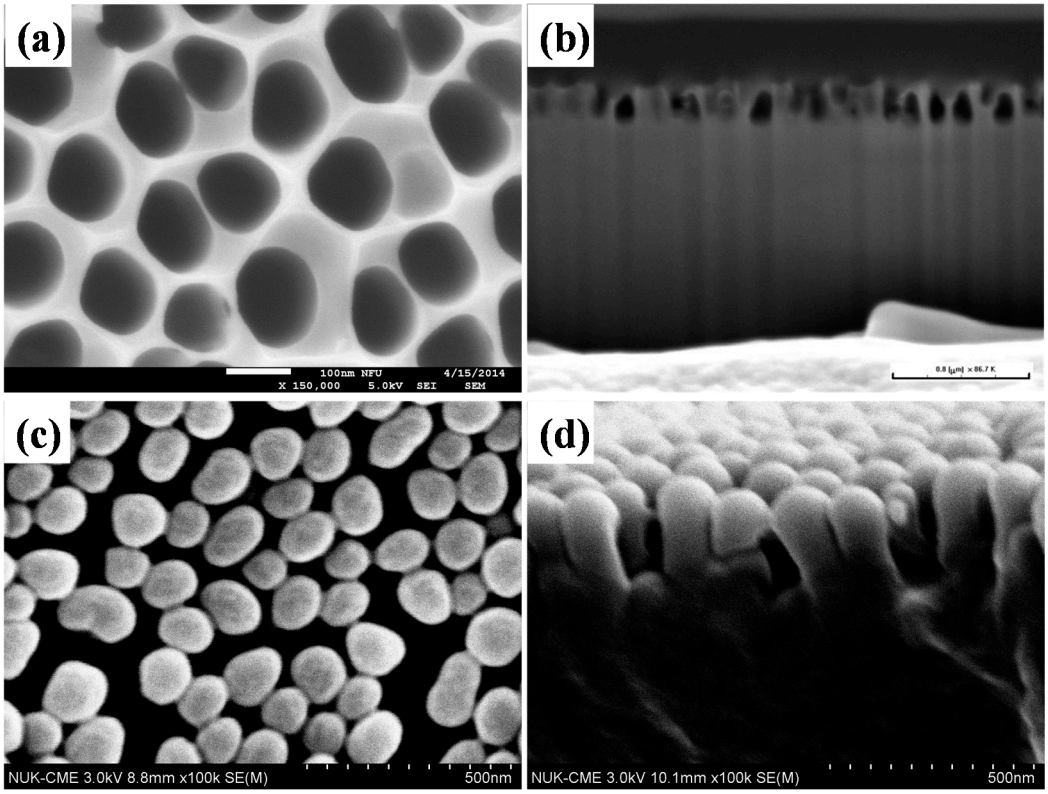

Figure 2. FE-SEM top-view and cross-sectional of AAO template and PMMA film with sub-wavelength moth-eye structures. (**a**) and (**b**) top-view and cross-sectional of AAO template; (**c**) and (**d**) top-view and cross-sectional of PMMA film with sub-wavelength moth-eye structures.

In order to verify the transmittance of our new designed AR film. Three different structures of AR film were tested. The transmittance of bare glass (sample A) were also characterized for control. The three different AR films are PDMS/glass (sample B), flat PMMA/PDMS/glass (sample C) and moth-eye structured PMMA/PDMA/glass (sample D). Figure 3 shows results of transmittance versus wavelength of the four samples. The four transmittance data at wavelength of 550 nm are also listed in Table I. Coating PDMS on glass would enhance the transmittance since refractive index of PDMS is 1.42 which is in between glass (1.53) and air (1.00). Thus comparing sample A with sample B the transmittance improve 4.47%, increasing from 79.27% to 83.74%. With additional flat PMMA film attached on PDMS/glass (sample C) the transmittance drop from 83.74% to 80.22% due to the refractive index of PMMA is slightly higher than that of PDMS which may cause light reflection at interface between PDMS and PMMA. With the moth-eye structured PMMA film attached on PDMS/glass (sample D) the transmittance increases up to 84.58% which is the highest value among four samples with 5.31% improving if comparing to that of bare glass. The results indicate that new

Peer-reviewed version available at Materials 2017, 10, 296; doi:10.3390/ma10030296

designed subwavelength moth-eye structured PMMA film indeed enhance the amount of light that penetrating into the DSSC.

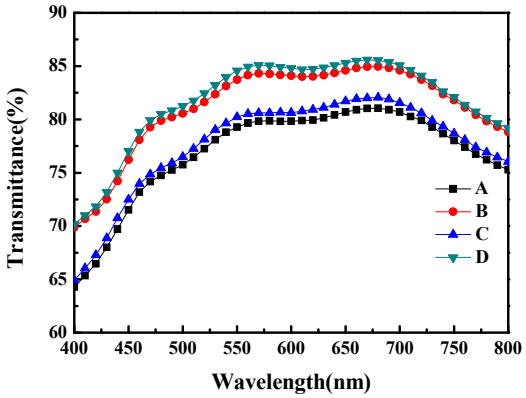

Figure 3. The UV-Vis transmittance spectra. Curves from A to D represent transmittances of bare glass (**sample A**), PDMS/glass (**sample B**), flat PMMA/PDMS/glass (**sample C**) and sub-wavelength moth-eye structured PMMA/PDMS/glass (**sample D**), respectively.

The four samples then further assembled to become DSSC devices. Electrochemical impedance spectroscopy was being employed to further understanding the electron transfer processes in the DSSC. Figure 4 shows the Nyquist plots of sample A to D. Three distinct semicircles are observed in the frequency range of 10 mHz–100 kHz, which are attributed to, from left to right, the electrochemical reaction at the Pt counter electrode and electrolyte interface, charge transport through the TiO_2/dye/electrolyte interface, and the Warburg diffusion process of I^-/I^{3-} in the electrolyte, respectively [18,19]. The diameter of the left semicircle refers to the electrical resistance (RPt) at the Pt counter electrode/electrolyte interface. Figure 3 shows that RPt of the four samples are similar, indicating that the DSSC fabricating process is stable. The diameter of the middle semicircle corresponds to the recombination resistance (Rrec) associated with the transport of electrons through the dye/TiO_2 NPs photoanode/electrolyte interfaces. The right semicircle represents the resistance of I^{3-} ions diffusion in the electrolyte, denoted as RD [20]. The results of RK and RD of the four samples are listed in Table 1. The minimum RK of 9.6 Ω was observed for the DSSC with subwavelength moth-eye structured PMMA AR film top on it. This is because the film enhances penetration of incident light into dye layer resulting in producing more excited electron-and-hole pairs than those without the film. In other words, the film facilitates high carrier density in the DSSC working area. Though the mobility of the carriers may keep the same, the resistivity of specific charge transfer is reduced.

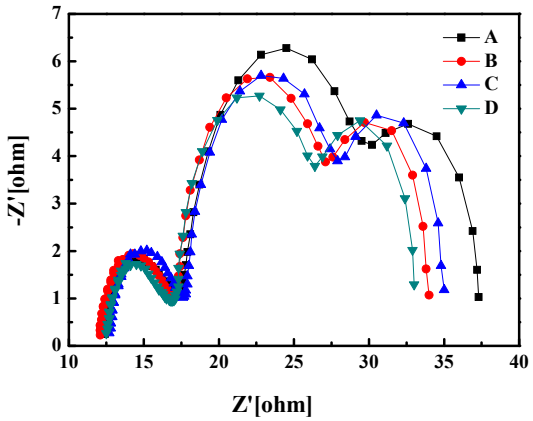

Figure 4. Nyquist plots of the DSSCs. Curves from A to D represent impedance of bare glass (**sample A**), PDMS/glass (**sample B**), flat PMMA/PDMS/glass (**sample C**) and sub-wavelength moth-eye structured PMMA/PDMS/glass (**sample D**), respectively.

Peer-reviewed version available at Materials 2017, 10, 296; doi:10.3390/ma10030296

Figure 5 shows incident monochromatic photon-to-current conversion efficiency (IPCE) as a function of wavelength of the four samples. The wavelength ranges from 300 to 800 nm. The IPCE represents number of electron-and-hole pairs that can be generated by monochromatic incident light per unit time. Among four samples, sample D which has moth-eye structured PMMA AR film shows highest IPCE value of 66.2%. Comparing the value to that of sample A, the IPCE significantly increases 8.7% (from 60.9% to 66.2%). The results imply that sample D has highest carrier density among four samples, which is consistent with the minimum Rrec observed in the electrochemical impedance spectroscopy.

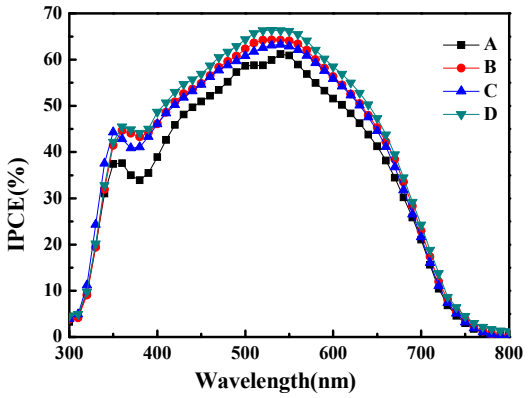

Figure 5. IPCE characteristics of the DSSCs. Curves from A to D represent Incident monochromatic Photon-to-current Conversion Efficiency of bare glass (**sample A**), PDMS/glass (**sample B**), flat PMMA/PDMS/glass (**sample C**) and sub-wavelength moth-eye structured PMMA/PDMS/glass (**sample D**), respectively.

Figure 6 shows current density (J) versus voltage (V) characteristics of sample A to D measured under AM 1.5G illumination at 100 mW/cm^2. The open-circuit voltage (VOC) and short-circuit current density (JSC) of the four samples are listed in Table I. The open-circuit voltage (VOC) is similar among four samples. The short-circuit current density (JSC), however, increases from 14.77 mA/cm^2 (sample A) to 15.62 mA/cm^2 (sample B) with attaching PDMS AR layer. The JSC is further improved to 15.79 mA/cm^2 (Sample D) by attaching additional sub-wavelength moth-eye structured PMMA film on sample B.

Based on the J-V characteristics, the energy conversion performances of sample A to D were calculated and are also summarized in Table 1. Comparing sample A with sample B, the energy conversion efficiency (η) increases from 6.26% to 6.41% due to the effect of PDMS AR layer. Comparing sample A with sample D the energy conversion efficiency (η) increases from 6.26% to 6.79%. Thus comparing sample B and D the energy conversion efficiency (η) is improved by 5.93% only with attaching an additional sub-wavelength moth-eye structured PMMA AR film on PDMS layer. Sample C which attached a flat PMMA film on PDMS layer has relatively low energy conversion efficiency of 6.33% because the flat PMMA film could not effectively enhance the light transmittance. In overall, Sample D shows the highest energy conversion efficiency of 6.79%.

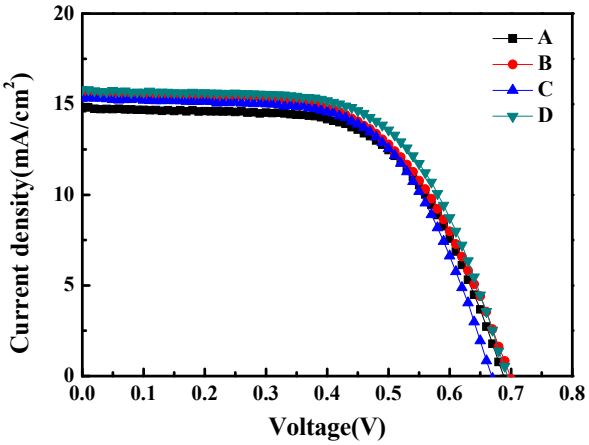

Figure 6. Current density (J) versus voltage (V) characteristics of the DSSCs. Curves from A to D represent J-V curve of bare glass (**sample A**), PDMS/glass (**sample B**), flat PMMA/PDMS/glass (**sample C**) and sub-wavelength moth-eye structured PMMA/PDMS/glass (**sample D**), respectively.

Table 1. Characteristics of DSSCs fabricated on the FTO glass.

Sample	Transmittance@550 nm (%)	V_{OC} (V)	J_{SC} (mA/cm^2)	F.F (%)	η (%)	R_{rec} (Ω)	R_D (Ω)
A	79.27	0.69	14.77	61.55	6.26	12.9	7.1
B	83.74	0.70	15.62	58.79	6.41	10.2	6.9
C	80.22	0.67	15.31	61.83	6.33	10.3	7.1
D	84.58	0.69	15.79	61.90	6.79	9.6	6.6

4. Conclusions

In this study the DSSC attached with double anti-reflection (AR) layer composed of a subwavelength moth-eye structured PMMA film and a PDMS film were fabricated. The subwavelength moth-eye structured PMMA film was proved to enhance light penetration into DSSC working area. The light transmittance is enhanced by 5.31% and 4.47% for the case of double AR layer (subwavelength moth-eye structured PMMA film/PDMS) and PDMS film along when comparing with bare glass, respectively. The double AR layer DSSC shows the IPCE value of 66.2% at the wavelength of 550 nm, which is 8.7% higher than that of DSSC without any AR layer. The internal impedance reduces from 12.9 Ω to 9.6 Ω, the short-circuit current density increased from 14.77 to 15.79 and the photoelectric conversion efficiency increase from 6.26% to 6.79% when comparing the DSSC without AR layer with that with double AR layer, respectively. More important, the process to fabricate DSSC device with double AR layer composed of subwavelength moth-eye structured PMMA/PDMS is compatible with the high pressure mechanical compression technology and the high temperature annealing process.

Acknowledgments: The authors would like to thank Teen Hang Meen, Tian Chiuan Wu, Tung Lung Wu, Jyun-Yang Tang, and Cheng-Fu Yang for their assistance. The project was supported by the Ministry of Science and Technology of Taiwan for financially supporting this work under contract No. MOST 103-2112-M-150-002 and No. MOST 104-2112-M-150-002. We also grateful to the Core Facilities Laboratory in Kaohsiung-Pingtung area for their help.

Author Contributions: T.J.K. designed this work, analyzed the results and wrote this manuscript. Y.S.T. carried out the preparation of samples and measurements. All authors read and approved the final manuscript.

Conflicts of Interest: The authors declare no conflict of interest.

References

1. Chen, J.Y.; Chang, W.L.; Huang, C.K.; Sun, K.W. Biomimetic nanostructured antireflection coating and its application on crystalline silicon solar cells. *Opt. Express* **2011**, *19*, 14411–14419.
2. Chiu, M.Y.; Chang, C.H.; Tsai, M.A.; Chang, F.Y.; Yu, P. Improved optical transmission and current matching of a triple-junction solar cell utilizing sub-wavelength structures. *Opt. Express* **2010**, *18*, A308–A313.
3. Kanamori, Y.; Roy, E.; Chen, Y. Antireflection sub-wavelength gratings fabricated by spin-coating replication. *Microelectron. Eng.* **2005**, *78–79*, 287–293.
4. Doshi, P.; Jellison, G.E.; Rohatgi, A. Characterization and optimization of absorbing plasma-enhanced chemical vapor deposited antireflection coatings for silicon photovoltaics. *Appl. Opt.* **1997**, *36*, 7826–7837.
5. Kuo, M.L.; Poxson, D.J.; Kim, Y.S.; Mont, F.W.; Kim, J.K.; Schubert, E.F.; Lin, S.Y. Realization of a near-perfect antireflection coating for silicon solar energy utilization. *Opt. Lett.* **2008**, *33*, 2527–2529.
6. Macdonald, D.H.; Cuevas, A.; Kerr, M.J.; Samundsett, C.; Ruby, D.; Winderbaum, S.; Leo, A. Texturing industrial multicrystalline silicon solar cells. *Sol. Energy* **2004**, *76*, 277–283.
7. Jiao, F.; Huang, Q.; Ren, W.; Zhou, W.; Qi, F.; Zheng, Y.; Xie, J. Enhanced performance for solar cells with moth-eye structure fabricated by UV nanoimprint lithography. *Microelectron. Eng.* **2013**, *103*, 126–130.
8. Shin, B.K.; Lee, T.I.; Xiong, J.; Hwang, C.; Noh, G.; Cho, J.H.; Myoung, J.M. Bottom-up grown ZnO nanorods for an antireflective moth-eye structure on $CuInGaSe_2$ solar cells. *Sol. Energy Mater. Sol. Cells* **2011**, *95*, 2650–2654.
9. O'Regan, B.; Grätzel, M. A low-cost, high-efficiency solar cell based on dye-sensitized colloidal TiO_2 films *Nature* **1991**, *353*, 737–740.
10. Ting, C.J.; Huang, M.C.; Tsai, H.Y.; Chou, C.P.; Fu, C.C. Low cost fabrication of the large-area anti-reflection films from polymer by nanoimprint/hot-embossing technology. *Nanotechnology*, **2008**, *19*, doi:10.1088/0957-4484/19/20/205301.
11. Han, K.S.; Shin, J.H.; Yoon, W.Y.; Lee, H. Enhanced performance of sola rcells with anti-reflection layer fabricated by nano-imprint lithography. *Sol. Energy Mater. Sol. Cells* **2011**, *95*, 288–291.
12. Kim, M.K.; Yi, D.K.; Paik, U. Tunable, Flexible Antireflection Layer of ZnO Nanowires Embedded in PDMS. *Langmuir* **2010**, *26*, 7552–7554.
13. Chen, H.C.; Lin, C.C.; Han, H.V.; Chen, K. J.; Tsai, Y.L.; Chang, Y.A.; Shih, M.H.; Kuo, H.C.; Yu, P. Enhancement of power conversion efficiency in GaAs solar cells with dual-layer quantum dots using flexible PDMS film. *Sol. Energy Mater. Sol. Cells* **2012**, *104*, 92–96.
14. Chen, J.Y.; Sun, K.W. Enhancement of the light conversion efficiency of silicon solar cells by using nanoimprint anti-reflection layer. *Sol. Energy Mater. Sol. Cells* **2010**, *94*, 629–633.
15. Meen, T.H.; Tsai, J.K.; Tu, Y.S.; Wu, T.C.; Hsu, W.D.; Chang, S.J. Optimization of the dye-sensitized solar cell performance by mechanical compression. *Nanoscale Res. Lett.* **2014**, *9*, doi:10.1186/1556-276X-9-523.
16. Tsai, J.K.; Hsu, W.D.; Wu, T.C.; Meen, T.H.; Chong, W.J. Effect of compressed TiO_2 nanoparticle thin film thickness on the performance of dye-sensitized solar cells. *Nanoscale Res. Lett.* **2013**, *8*, doi:10.1186/1556-276X-8-459.
17. Tsai, J.K.; Hsu, W.D.; Wu, T.C.; Zhou, J.S.; Li, J.L.; Liao, J.H.; Meen, T.H. Dye-Sensitized Solar Cells with Optimal Gel Electrolyte Using the Taguchi Design Method. *Int. J. Photoenergy* **2013**, *2013*, doi:10.1155/2013/617126.
18. Wang, Q.; Moser, J.E.; Grätzel, M. Electrochemical Impedance Spectroscopic Analysis of Dye-Sensitized Solar Cells. *J. Phys. Chem. B* **2005**, *109*, 14945–14953.
19. Adachi, M.; Sakamoto, M.; Jiu, J.; Ogata, Y.; Isoda, S. Determination of Parameters of Electron Transport in Dye-Sensitized Solar Cells Using Electrochemical Impedance Spectroscopy. *J. Phys. Chem. B* **2006**, *110*, 13872–13880.
20. Raga, S.R.; Barea, E.M.; Fabregat-Santiago, F. Analysis of the Origin of Open Circuit Voltage in Dye Solar Cells. *J. Phys. Chem. Lett.* **2012**, *3*, 1629–1634.